scientific reports

Check for updates

OPEN

How modulation of the tumor microenvironment drives cancer immune escape dynamics

Pujan Shrestha[1,2], Zahra S. Ghoreyshi[1,2] & Jason T. George[1,2,3]✉

Metastatic disease is the leading cause of cancer-related death, despite recent advances in therapeutic interventions. Prior modeling approaches have accounted for the adaptive immune system's role in combating tumors, which has led to the development of stochastic models that explain cancer immunoediting and tumor-immune co-evolution. However, cancer immune-mediated dormancy, wherein the adaptive immune system maintains a micrometastatic population by keeping its growth in check, remains poorly understood. Immune-mediated dormancy can significantly delay the emergence (and therefore detection) of metastasis. An improved quantitative understanding of this process will thereby improve our ability to identify and treat cancer during the micrometastatic period. Here, we introduce a generalized stochastic model that incorporates the dynamic effects of immunomodulation within the tumor microenvironment on T cell-mediated cancer killing. This broad class of nonlinear birth-death model can account for a variety of cytotoxic T cell immunosuppressive effects, including regulatory T cells, cancer-associated fibroblasts, and myeloid-derived suppressor cells. We develop analytic expressions for the likelihood and mean time of immune escape. We also develop a method for identifying a corresponding diffusion approximation applicable to estimating population dynamics across a wide range of nonlinear birth-death processes. Lastly, we apply our model to estimate the nature and extent of immunomodulation that best explains the timing of disease recurrence in bladder and breast cancer patients. Our findings quantify the effects that stochastic tumor-immune interaction dynamics can play in the timing and likelihood of disease progression. Our analytical approximations provide a method of studying population escape in other ecological contexts involving nonlinear transition rates.

Keywords Cancer immunotherapy, Mathematical Oncology, Applied stochastic processes, Diffusion approximation

Metastatic disease remains the top contributor to cancer mortality despite the continued development of improved therapies. A large body of stochastic modeling and empirical work has established mechanisms of primary cancer progression via pre-existent and acquired resistance, through which therapeutic intervention commonly results in the evolutionary selection of resistant populations[1–5]. Recent strides in cancer treatment have been made by enhancing the anti-tumor capacity of the adaptive immune system[6]. In this context, experimental investigation and complementary stochastic models have been developed to study cancer immunoediting, explain cancer incidence[7–10], and correlate observed evolutionary patterns of disease with tumor-immune co-evolution[11–17].

Immune-mediated cancer dormancy, in contrast, represents a distinct and understudied problem related to cancer metastatic control. Early on, tumor cells extravasate from the primary disease site into circulation, where they can then ultimately settle at distant metastatic locations[18]. The maintenance of actively growing cell populations at small sizes with balanced cell death represents one mechanism through which time to metastasis can be substantially prolonged[19,20].

As with primary disease, micrometastatic cancer populations are also subjected to immunoediting by the adaptive immune system, wherein appreciable disease proceeds through elimination, equilibrium, and escape phases[21]. Disruptions to balanced cancer growth and T cell killing in immune-mediated dormancy can result in clinically appreciable disease. In two unfortunate clinical cases, kidney transplant recipients from a shared donor with prior history of primary melanoma developed either secondary melanoma at the kidney site or subcutaneous melanoma, likely as a result of their transplant-specific immunosuppressive regimen[22]. In separate

[1]Department of Biomedical Engineering, Texas A&M University, College Station, TX 77843, USA. [2]Translational Medical Sciences, Texas A&M Health Science Center, Houston, TX 77030, USA. [3]Center for Theoretical Biological Physics, Rice University, Houston, TX 77005, USA. ✉email: jason.george@tamu.edu

studies, carcinogen-injected mice that did not develop progressive malignancy with stable masses at the injection site were treated with control antibody or antibody-depleting T cells[23]. In contrast with the control group, mice treated with T cell immune-depleting therapy developed progressive malignancy, and a repeated experiment with mice lacking adaptive immunity resulted in very few late-forming tumors, further implicating the role of T cell immunity in the long-term maintenance of cancer equilibrium[24].

Anti-tumor T cell responses can also be significantly affected by the presence of immunomodulatory elements in the tumor microenvironment. Immunomodulation is complex and involves a variety of chemical and cellular inputs. For example, cancer and stromal cells deprive T cells of nutrients, thereby encouraging exhaustion[25]. Regulatory T cells (Tregs) and cancer-associated fibroblasts (CAFs) accumulate in the microenvironment and inhibit T cells directly and indirectly[26–30]. MDSCs expand and contract with tumor size, and have been shown to sequester cysteine from T cells and contribute to the presence of Tregs[31–35].

The near-impossibility of long-term clinical studies tracking micrometastatic initiation and growth necessitates a mathematical modeling framework capable of evaluating the timing and likelihood of cancer immune-mediated dormant resurgence as a function of dynamical signals and cell types in the metastatic immune microenvironment. Prior models have been proposed to study immune-mediated dormancy, including ODE models of tumor-immune interactions[36,37]. These models, while capable of describing mean behavior, characterize cell sizes on a continuum, and so scenarios involving equilibrium population sizes that are close to zero neglect the nontrivial extinction probability of this absorbing state and thus susceptibility to stochastic fluctuations. The incorporation of active immunomodulation provides an Allee effect that can drive cancer growth at very small population sizes. Despite this, the failure of ODE models to account for the random fluctuations in population size that may drive the system away from a stable equilibrium point and ultimately into escape or elimination necessitated the development of a stochastic modeling framework. The stochastic birth-death framework and its associated diffusion approximation are more complicated models, but are well positioned to quantify the likelihood and mean time of population escape and elimination.

To address the above questions and current limitations, we develop a generalized stochastic modeling framework that incorporates the effects of dynamical immunomodulatory cells present in the microenvironment. We construct a nonlinear birth-death model, wherein immunomodulatory regulation of effector T cells impairs their cancer killing ability. When applied to clinical data on cancer progression, our model predicts that the timing and likelihood of breast and bladder cancer is best explained by a microenvironment that varies dynamically with respect to the tumor burden. We also develop a diffusion approximation sufficiently general to handle reasonable assumptions on nonlinear birth-death processes, which we anticipate will be of broad use for additional applications that involve the description of nontrivial per-capita death rates.

Material and methods

Model development

Our model considers a small dividing cancer population experiencing linear growth and active killing by cytotoxic (CD8+) T cells . We assume that the cancer cells exhibit exponential growth and that robust immune responses are capable of imparting a high per-cell death rate on cancer cells, even at large tumor sizes, which can lead to cancer elimination. That would be the whole story, except that T cell killing rates can be diminished by exogenous factors in the tumor microenvironment. This necessarily requires a dynamical model capable of accounting for diversity in the microenvironmental influences on T cell killing rates, resulting from neighboring passive and actively immunoinhibitory cells (Fig. 1A).

We account for possible reductions in the T cell killing rate by introducing an *immunomodulation function* f that depends on tumor size n and the abundance of immunoinhibitory agents M. In general, we model these effects via the transition rates for the underlying birth-death process representing the tumor population. Namely, the birth and death transition rates are given by

$$\lambda_n = rn; \qquad \mu_n = \delta n f(n; M). \tag{1}$$

respectively where r, δ with $\delta >> r$ are cancer per-capita growth and death rates, respectively. Here, $f(n; M)$ is the immunomodulation function. $f \leq 1$ accounts for reductions in the T cell killing rate via M inhibitory cells. We consider both cases where M is constant or dynamic with respect to tumor size, and we refer to these as *static* and *dynamic immunomodulatory landscapes*, respectively. Refer to Sec. S8.2 of the SI for a general framework for the landscapes. We note that while there exist many reasonable choices for the precise functional form of f, for foundational understanding, we consider several specific cases below.

Static immunomodulatory landscape

In the simplest case, we assume that the tumor is surrounded by a fixed number of M neighboring stromal (nonmalignant) cells whose presence passively impairs T cell killing by diluting meaningful cancer-T cell interactions. We call this case *passive immunomodulation* with the functional form of f given by

$$f_p(n; M) = \frac{n}{n + M}. \tag{2}$$

Here, $f \leq 1$ reduces baseline T cell killing. We will show that T cell impairment via the mere presence of passive neighboring cells is incompatible with possible tumor escape. Furthermore, passive immunomodulation does not account for situations where the tumor microenvironment itself is immunosuppressive. For example, previous

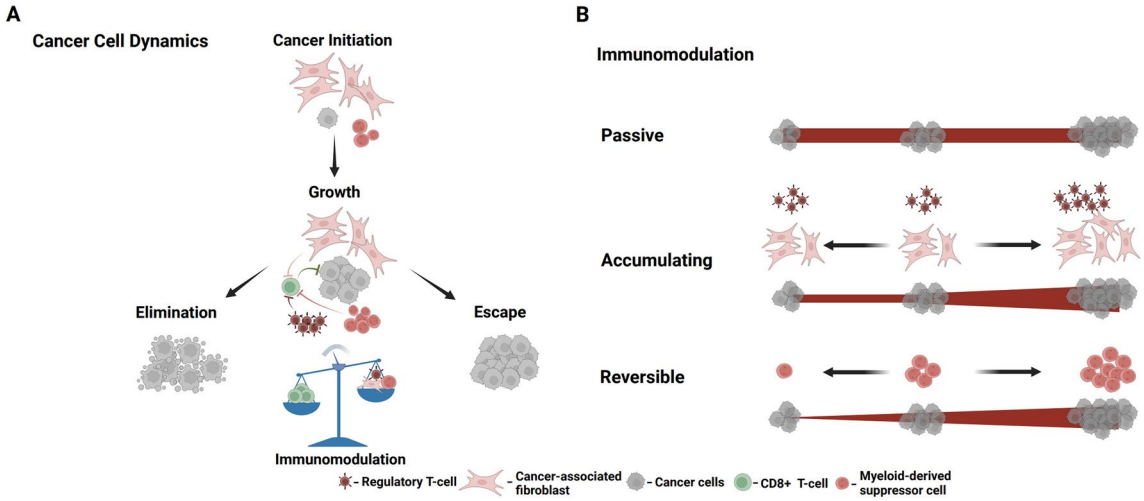

Fig. 1. (**A**) Conceptual schematic illustrating the tumor-immune dynamics that would lead to elimination or escape for the tumor population. The scale represents the relative balance between recognizing effector T cells, which eliminate the cancer, and the immunomodulatory factors that can diminish T cell killing and lead to immune escape. (**B**) Immunomodulatory cells in the tumor microenvironment can act to impair T cell killing in a variety of ways. In the simplest "passive" case, the number of immunomodulatory cells is assumed to be fixed and independent from the number of cancer cells (M constant). Alternatively, the number of immunomodulatory cells may vary as a function of cancer cell number. In the "accumulating" case, the largest size that tumor population reaches determines M. This immunomodulation models the effects of Tregs and cancer-associated fibroblasts. In contrast, "reversible" immunomodulation describes the case in which the number of immunomodulatory cells may grow and shrink as a function of the number of cancer cells. This case may be more appropriate for modeling myeloid-derived suppressor cells. Created with BioRender.com.

studies have suggested that T cell function is further impaired via metabolic dysfunction[38]. Tumor cells together with glucose-depleted and lactate-rich environments can also lead to enhanced Treg suppressor activity[39].

We thus expand our model to consider *active immunomodulation*, wherein both the tumor cells and the neighbouring cells can modulate the level of T cell impairment. We list one such functional form wherein the death rate is inversely proportional to a linear combination of the inhibition signal and the tumor size. In this active case,

$$f_a(n;M) = \left(\frac{n}{M+n}\right)\left(\frac{1}{\alpha M + \beta n}\right), \tag{3}$$

where α and β represent the effects induced by both types of cells in the tumor microenvironment. In order to avoid death amplification effects, we only consider positive values for α and β for the remainder of the text.

Dynamic immunomodulatory landscape

Of course, it is also possible that immunomodulatory cells may vary dynamically with respect to the number of cancer cells. We also consider the more general scenario where changes in M are induced by changes in the tumor size. Motivated by cases where the growing tumor cells permanently recruit neighboring stromal cells[40] and also the reversible impact of MDSCs[35], we describe two distinct dynamical behaviors: one where the inhibitory signal, M, increases and decreases in response to the tumor population, and the other where immunoinhibitory signals depend on the cancer population size and, once present, exist permanently. We refer to these cases as *reversible* and *accumulating* immunomodulation, respectively (Fig. 1B), and we calculate tumor escape probabilities in these settings from an analytical perspective as well as a computationally tractable method. To that end, we consider a large size, N representing tumor escape and compute the probabilities that the tumor population, $0 < n < N$, ultimately hits the tumor escape size while avoiding tumor elimination.

Diffusion approximation

We construct a diffusion approximation of the birth-death process to further verify the results of the passive immunomodulation case with the understanding that the mathematical framework thus demonstrated applies to a larger class of birth-death processes. We show that if the mean and variance expression for the birth-death model are Lipschitz, then one can find a diffusion approximation represented by a stochastic differential equation. We will establish a generalized approach for identifying a diffusion approximation represented by a stochastic

differential equation for the broad class of birth-death processes whose mean and variance are Lipschitz. Using this approximation, we employ the full range of the Itô calculus to obtain closed-form expressions for absorption probabilities as well as the mean absorption times where absorption refers to the event that the tumor population starting away from zero gets absorbed to zero (tumor elimination) or to the tumor escape size.

Numerical simulation

All analytical results are compared to large-scale stochastic numerical simulation via the Gillespie algorithm.

Data analysis

Lastly, we apply these findings to cancer incidence data for patients from diagnosis to first progression, first progression to second progression, and so on to estimate the immunomodulation parameters from each event interval. In absence of clinical micrometastasis longitudinal tumor trajectory data, we characterize immune escape relative to individual progression events. We then calculate the distribution for progression time and subsequently fit our model. Best fit parameters were selected based on minimizing the mean squared error for the distribution of progression times for each progression event and for each cancer case. The breast cancer data was obtained from the website[41] associated with the breast cancer forecasting work by Newton et al.[42] using clinical data from Memorial Sloan Kettering Cancer Center and MD Anderson Cancer Center. Similarly, the bladder cancer data was obtained from the website[43] associated with the modelling work by Hasnain et al.[44] using clinical data from USC Institute of Urology.

Results

In the following, we present the main findings of our analysis. Full mathematical derivations are provided in the Supplementary Information (SI). An overview is provided in SI Sec. S1. For the purposes of this section, n represents the integer values attained by the birth death process and x represents its continuous version.

Passive immunomodulation alone cannot promote cancer escape

If immune recognition is passively diminished by the presence of M neighboring nonmalignant cells as in (2), then the net growth rate, $\xi(x) \triangleq \lambda_x - \mu_x$, is given by

$$\xi(x) = \left(r - \frac{\delta x}{M + x}\right) x. \tag{4}$$

This behavior yields one unstable equilibrium point at the origin and one stable equilibrium point at $x^* = rM/(\delta - r)$ (Fig. 2A). Moreover, as a sequence of functions, the $\xi(x)$ are increasing with respect to the inhibitory element M. The mean elimination time for this process, $\mathbb{E}[T_0]$ (see SI Sec. S4), satisfies:

$$\mathbb{E}[T_0] < \frac{1}{(1 - r/\delta)^{M+1}} < \infty. \tag{5}$$

Collectively, these dynamics predict that under passive immunomodulation the population cannot grow to an arbitrarily large size but instead will fluctuate around x^* (Fig. 2B). However, the stochasticity of the birth-death process ultimately results in disease elimination after a finite average waiting time. $\xi(x) > 0$ for $x < x^*$, which creates an barrier to elimination, and because ξ is an increasing function of M this barrier also increases as M grows, resulting in larger elimination times.

Under this model, appreciable disease only occurs if $x^* \gg 1$, which, for effective T cell killing rates ($\delta - r > r$), requires M to be many multiples larger than the size of macroscopically detectable disease. This finding, together with the absence of cancer escape, suggests passive immunomodulation alone is insufficient for explaining observed dynamics.

Diffusion approximation for general nonlinear birth-death processes

Despite its simplicity, the above case presents a prototypical example of a nonlinear birth-death model wherein we desire statistical characterizations of escape for processes that can grow to large sizes prior to reaching an absorption state. Motivated by a desire to develop analytically tractable estimates of elimination probabilities and mean escape times for a variety of birth-death processes, we next developed a general diffusion approximation-based approach.

Consider a birth-death process $X^N(t)$ on a state space $\{0, 1, \cdots, N\}$ for $N \gg 1$ representing the absorption size at cancer escape, with transition rates given by (1). Then we can construct an approximation $Z^N(t)$ defined by the stochastic differential equation:

$$\begin{cases} dZ^N(t) = \frac{1}{\sqrt{N}} \sqrt{G(Z^N(t))} dW(t) + F(Z^N(t))dt \\ Z^N(0) = x_0 \in [0, 1], \end{cases} \tag{6}$$

where $W(t)$ is a standard Brownian motion, $F(x) = \lambda_x - \mu_x$ and $G(x) = \lambda_x + \mu_x$. Note that, $Z = X/N$ tracks the population ratio with $Z = 1$ corresponding to cancer escape. We calculate the closed-form solution

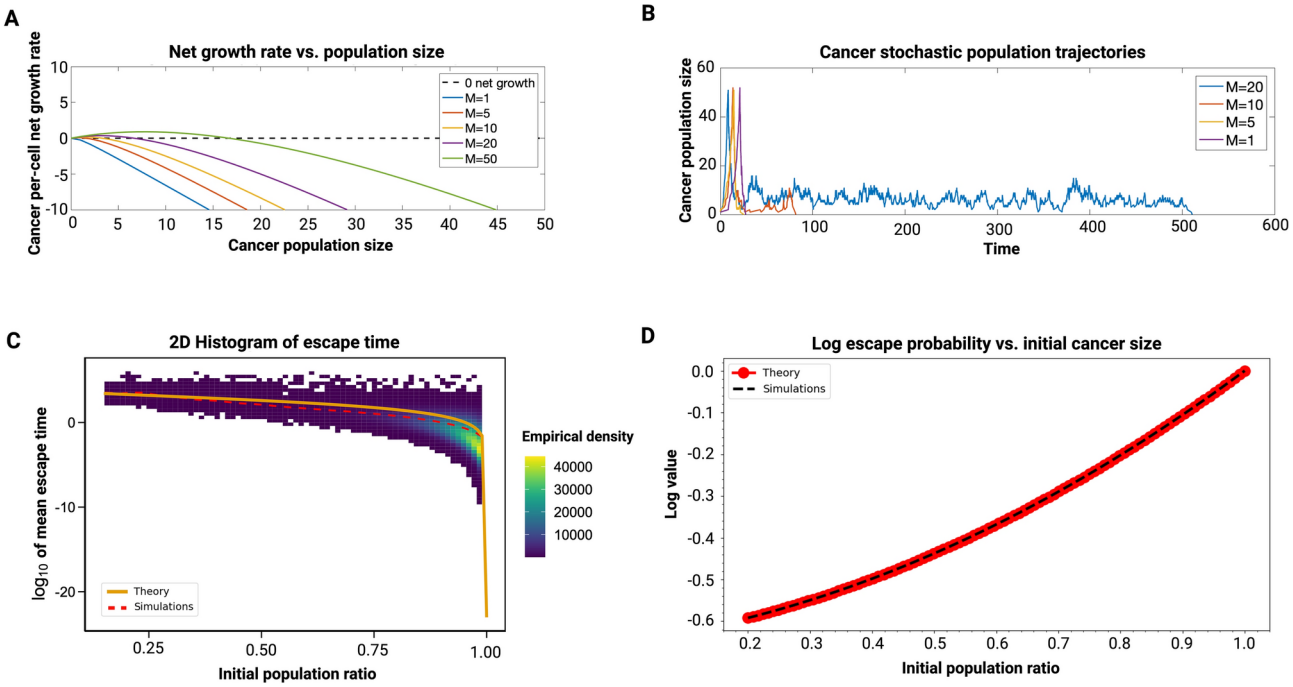

Fig. 2. Dynamics under passive immunomodulation. (**A**) Schematic of the cancer per-cell net growth rate as a function of cancer population size for various levels of immunomodulation ($r = 0.25$, $\delta = 1$). (**B**) Simulated stochastic trajectories with various immunomodulatory parameters ($r = 0.25$, $\delta = 1$). Results of largescale stochastic simulations and analytical estimates for the diffusion approximation are provided for cancer population (**C**) mean escape time and (**D**) escape probability. The diffusion approximation for passive immunomodulation is given as a function of initial population ratio with $r = 0.1$, $\delta = 0.8$, $N = 100$, and $M = 2$. Total simulations for initial population ratio under and over 0.25 are 100, 000 and 10, 000, respectively. Dashed lines represent simulated values and solid lines represent the analytical result obtained via diffusion approximation.

Model	$f(n; M)$	Equilibrium Points, Stability, and Dynamics
Passive	$\frac{n}{n+M}$	$x_1^* = 0$, unstable, escape. $x_2^* > 0$, stable, dormancy.
Product	$\left(\frac{n}{M+n}\right)\left(\frac{1}{\alpha M \cdot \beta n}\right)$	$x^* = 0$, unstable, escape or, $x_1^* = 0$, stable, dormancy and $x_2^* > 0$, unstable.
Linear	$\left(\frac{n}{M+n}\right)\left(\frac{1}{\alpha M+\beta n}\right)$	$x^* = 0$, unstable, escape or, $x_1^* = 0$, stable, dormancy with $x_2^* > 0$, unstable, or $x_1^* < x_2^*$, where: $x_1^* > 0$, stable, dormancy. $x_2^* > x_1^*$, unstable, escape.

Table 1. Summary of inhibition models with respective equilibrium points, stability, and dynamics.

for ultimate extinction probability and time to escape given the initial population ratio x_0. Let $U_0(x_0)$ to be the probability that the diffusion process is ultimately eliminated. It can be shown (SI Sec. S6.2) that,

$$U_0(x_0) = \frac{\Gamma(1-\alpha, \frac{\eta b}{c} + \eta x_0\,,\, \eta(\frac{b}{c}+1))}{\Gamma(1-\alpha, \frac{\eta b}{c}\,,\, \eta(\frac{b}{c}+1))}, \tag{7}$$

where α, b, η, c constants depend on N, M, δ , r, and Γ is the incomplete upper gamma function, given by

$$\Gamma(s, x, y) = \int_x^y t^{s-1} e^{-t} dt. \tag{8}$$

Similarly, if $\tau = \inf\{t > 0 \,|\, X(t) = 1\}$, then the mean time for escape (SI Sec. S6.3) can be shown the by given by

$$\mathbb{E}\left[\tau \mid X_0 = x_0\right] = -\int_{x_0}^{1}\int_{x_0}^{v} e^{-\int_v^y p(z)dz} dy\, r(v)dv. \tag{9}$$

Both of these closed-form equations are exact for the diffusion approximation. Our approximation well-represents the birth-death process across all initial population fractions whenever escape is assumed to occur at a large population size (in general, $N \sim 10^9$), as observed in comparing the analytical escape probability and mean time with those results obtained through largescale stochastic simulation (Fig. 2C-D). We remark that this approach can be applied identically to study a variety of nonlinear birth-death processes, with the general requirement that λ_x and μ_x are Lipschitz in population fraction to guarantee asymptotic agreement between the process and its diffusion approximation for large *N*. The passive case, while it allows for long periods of non-extinction, precludes any reasonable expectation for tumor immune escape at small population ratios. Collectively, these findings motivate the analysis of a more realistic model of immunomodulation's role in impairing T cell recognition.

Active immunomodulation permits both tumor elimination and escape

In the more general case, active immunomodulatory behavior may be modeled by accounting for additional impairments in T cell function that result from increases in the inhibitory signal *M* or total tumor cell size *n*. Such immunomodulation more accurately describes T cell dysfunction resulting from, for example, resource consumption (e.g., depletion of L-arginine or cystine), which can reduce T cell killing efficiency directly and increase Treg suppressor activity[38,39,45]. Such impairments can be accounted for by incorporating an additional term in the immunomodulation function that varies inversely with respect to cancer and immunomodulatory cell numbers. Toward this end, we considered a variety of possible functional forms (SI Sec. S7) and focus our main discussion here on one particular case that possessed representative dynamics. In this case, an additional $(\alpha M + \beta n)^{-1}$ term is added to the passive immunomodulation function (3) to account for reductions in the cancer per-capita T cell killing rates as a function of total cell abundance.

In systems employing the general dynamics given by Eq. (1), the asymptotic behavior $f_\infty = \lim_{n\to\infty} f(n)$ of the immunomodulatory function *f* can be partitioned by r/δ, which influences ultimate escape dynamics through the stability of the leading equilibrium point (See SI Sec. S5 for full details). Control occurs if $f_\infty < r/\delta$, while ultimate escape to large sizes occurs if $f_\infty > r/\delta$. In particular, passive immunomodulation yields $f_\infty = 1 > r/\delta$, resulting in stable cancer control, while active immunomodulation gives $f_\infty < r/\delta$, permitting cancer immune escape.

As such, the active immunomodulatory function f_a yields the size-inhomogeneous net-growth rate:

$$\xi(x) = rx - \delta x f_a(x; M) = rx - \frac{\delta x^2}{(M+x)(\alpha M + \beta x)}. \tag{10}$$

The nontrivial equilibrium points can be found by equating (10) to zero and solving

$$\beta x^2 + \left[(\alpha+\beta)\, M - \gamma\right] x + \alpha M^2 = 0, \quad for \;\; \gamma \equiv \delta/r > 1. \tag{11}$$

Since the above equation is quadratic in *x*, equilibrium points and their stability depend on the discriminant, $D(\alpha, \beta)$ of (11):

$$D(\alpha,\beta) = \left[\eta^2 - 2(\alpha+\beta)\eta + (\alpha-\beta)^2\right] M^2, \tag{12}$$

for $\eta \equiv \delta/rM$, where α (rsp. β) controls the strength of inhibition for every present inhibitory element (resp. cancer cell). If we re-normalize with respect to β, (11), and hence equilibria of (10), can be fully characterized by α. This affords a variety of variety of dynamical behavior (SI Sec. S7.2). The most interesting cases possess both stable and unstable equilibrium cell sizes (SI Fig. S3). We focus our subsequent analysis to this case.

Fig. 3 illustrate the behavior for the cancer net growth rate for various choices of the immunomodulatory parameter, *M*. The population regime of net-positive growth separating the origin from the first nonzero stable equilibrium state serves as a barrier to cancer elimination. Similarly, the population regime of net-negative growth rates above the first stable equilibrium population size to the population size of the nonstable equilibrium point represents a barrier to immune escape. Here, the stable and unstable states are separated by an activation barrier below which the population can be controlled by T cell recognition, and above which the microenvironment represses T cell killing enough to facilitate cancer escape. Hence a population existing at a stable equilibrium state would traverse either the elimination barrier to the left and become extinct, or it would cross the activation barrier to the right and undergo immune escape.

We remark that ξ is an increasing function of *M*, and so larger immunomodulaton leads to to larger equilibrium population sizes, larger elimination barriers, and reduced escape barriers. These dynamics allow a population to oscillate around the stable equilibrium for, perhaps large waiting times, prior to ultimate escape or elimination, and as a result more adequately model tumor-immune dynamics[21]. Additionally, this more general framework resembles passive immunomodulation in the regime of small *M*, where the leading unstable equilibrium, in general, can become comparable to the upper detection size, effectively preventing immune escape.

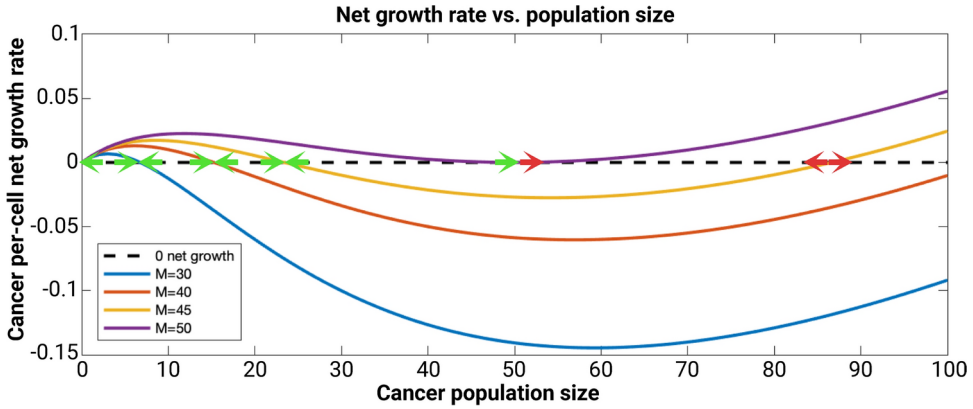

Fig. 3. Schematic for the cancer net growth rates under active immunomodulation. Increases in immune inhibition in the tumor microenvironment (via increases in M) lead to increases in the elimination barrier (values of the net growth curve from population size $n = 1$ until the first positive population size having zero net growth), and reduced barriers to immune escape (negative values of the net growth curve between the largest stable equilibrium point and detection size). In all cases, double green arrows indicate stable equilibrium points, double red arrows indicate unstable equilibrium points, and one of each indicates a semistable equilibrium point.

Dynamic immunomodulatory inhibition

Until now our model has assumed that the inhibitory signal, M, was constant throughout the evolution of the stochastic process. In reality, fluctuating cancer population sizes may also drive dynamic changes in immunomodulation present in the tumor microenvironment. For example, tumor-derived cytokines lead to Treg accumulation and can persist independent of tumor reduction[28]. Similarly, cancer-associated fibroblasts that persist even after large reductions in tumor size can promote cancer cell survival[29]. These examples would therefore be modeled more accurately assuming that immunomodulation *accumulates* as a tumor population grows, allowing for permanent recruitment of additional cells which remain the the tumor microenvironment irrespective of any future reductions in cancer size. Such a model contrasts with the behavior of myeloid-derived suppressor cells (MDSCs), another cell type capable of T cell impairment[32]. In this case, MDSCs are present in the tumor microenvironment, and empirical evidence has demonstrated that tumor removal leads to MDSC reduction, suggesting a *reversible* mechanism of immunomodulation[35] (See SI Sec. S2.1 for additional details). Motivated by these biological phenomena, we provide a further generalization of the above modeling framework capable of accounting for immunomodulatory parameters that vary dynamically as a function of the tumor size. To do so, we characterize the hitting and absorption probabilities.

Conditional hitting probabilities

Escape probability calculations are more involved in this case, since the level of immunomodulation at fixed population sizes now also depends on the dynamic variable M. To characterize immune escape probability, we first consider the probability that the cancer population reaches a particular size n starting from an initial size m conditional on not hitting size d, denoted by event ${}^{d}E_{n,m}$, for $d < m < n$. We first take an analytical approach to show that, for $n \geq d + 1$,

$$\mathbb{P}\left({}^{d}E_{n+1,n}\right) = \frac{D_{n-1}}{D_n}\nu_n, \qquad \text{with } \nu_n \equiv \frac{\lambda_n}{\lambda_n + \mu_n}. \tag{13}$$

The D_n in (13) is defined as a solution of the recursive relation, given by

$$D_{n+1} = D_n - \eta_n(1 - \eta_{n+1})D_{n-1}, \quad n \geq d + 2, \tag{14}$$

with $D_d = D_{d+1} = 1$. We identify the exact solution to this recursion relation (SI Sec. S8), however its implementation is computationally inefficient for large population sizes. For ease of calculations, we recast the recursion problem as a linear fractional transformation from real numbers to real numbers to evaluate the hitting probability by viewing it as a product of matrices. Namely,

$$\mathbb{P}\left({}^{d}E_{n+1,n}\right) = \frac{a\nu_{d+1} + b}{c\nu_{d+1} + e} \quad ; \begin{bmatrix} a & b \\ c & e \end{bmatrix} \triangleq \prod_{i=n}^{d+2} \begin{bmatrix} 0 & \nu_i \\ -\eta_i & 1 \end{bmatrix}. \tag{15}$$

To apply this machinery to our problem, we characterize the dynamics using two sequences: the first sequence $\{\delta_1, \delta_2, \dots\}$, $\delta_i \geq 0$ is a collection of cancer population sizes at which the value of M changes. $\{M_1, M_2, \dots\}$, $M_i \geq 0$ represents the corresponding immunomodulation values, so that $M = M_i$ whenever $\delta_i \leq X < \delta_{i+1}$. The birth and death rates used to calculate the relevant conditional probabilities are functions of both n and

M, given by $\lambda_{n,M}$ and $\mu_{n,M}$, respectively. We assume that the cancer population starts at initial size n_i with M_i suppressors. We remark that this framework is sufficiently general in its ability to handle any immune suppressor cell dynamics that can be represented by arbitrary $\{\delta_i\}$ and corresponding $\{M_i\}$ sequences.

Accumulating landscape

In this case, immunoinhibition M grows larger with increasing cancer population size and, once present, exists permanently. Thus, $M(t)$ increasing in time at every point that a new certain cancer population size threshold is achieved in the δ sequence. M is thus related to the maximal threshold size that the cancer population has currently achieved:

$$M(t) = M_{I(t)}; \quad I(t) = \max\left\{i \in \mathbb{Z} : \delta_i \leq \max_{0\leq\tau\leq t} X(\tau)\right\}. \tag{16}$$

Using this formulation, the probability of immune escape can be calculated as a function of "step-up" probabilities, which are the conditional hitting probabilities between adjacent values of the δ sequence. Namely,

$$P_{esc} = \mathbb{P}\left({}^0E_{\delta_{k^-}+1,1}\right) \prod_{k=k^-+1}^{\infty} \mathbb{P}\left({}^0E_{\delta_k+1,\delta_k}\right). \tag{17}$$

where k^- is the largest partition element such that $\delta_{k^-} \leq 1$. Using this approach, we calculate and compare the escape probabilities for the accumulating, reversible and the constant landscape using (13) and (15) (Fig. 4 and Fig. 5 respectively). Our results demonstrate that an accumulating landscape pushes the tumor population to explosion as the ability to irreversibly recruit more inhibitory cells further catalyzes cancer escape at larger sizes. The ultimate effect is a reduced escape barrier and more likely escape for comparable initial values for M.

Reversible landscape

In contrast with accumulating immunomodulation, reversible immunomodulation allows for M to both increase and decrease in response to cancer population growth and reduction, respectively. In this case, M is thus related to the current threshold size that the cancer has currently achieved in the δ sequence:

$$M(t) = M_{I(t)}; \qquad I(t) = \max\{i \in \mathbb{Z} : \delta_i \leq X(t)\}. \tag{18}$$

Largescale stochastic simulations for reversible and accumulating landscapes under a variety of partition intervals $\Delta = \delta_{i+1} - \delta_i$ were compared to our analytical calculations of escape probability, indicating excellent agreement (Fig. 5 and Figs. S7, S7, and S8 in the SI). Intriguingly, the reversible case experiences nonmonotonic behavior in cancer escape owing to the fact that M may reversibly decline during changes in tumor size. From the linear fractional transform approach using (15) (Fig. 4), our results demonstrate that the reversible landscape offers similar benefits to a growing tumor as the accumulating case thus also catalyzing cancer escape at larger sizes. However, the reversible decline in the immodulatory signal during tumor progression leads to a later escape as compared to the accumulating case. We achieve agreement between calculated and simulated values for both

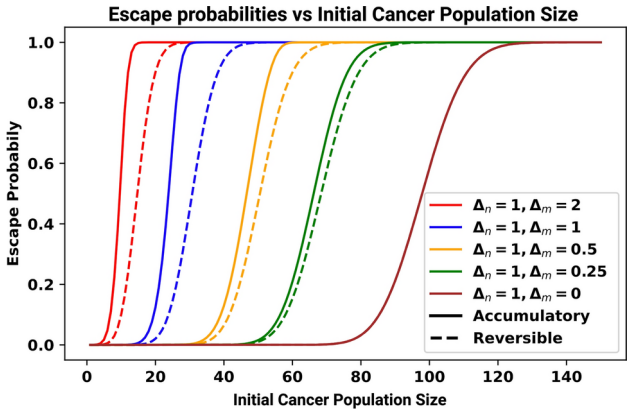

Fig. 4. Escape Probabilities obtained analytically under dynamic immunomodulatory landscapes. Every Δ_n change (increase for accumulating) in tumor size results in Δ_M change (increase resp.) in the immunomodulatory signal. The brown line ($\Delta_n = 1, \Delta_M = 0$) is a special case that represents the escape probability under constant immunomodulation. In all cases, f is used according to linear inhibition case in (3) with $r = 0.05, \delta = 0.9, N = 150, \alpha = 0.1, M_0 = 1, \beta = 0.18$.

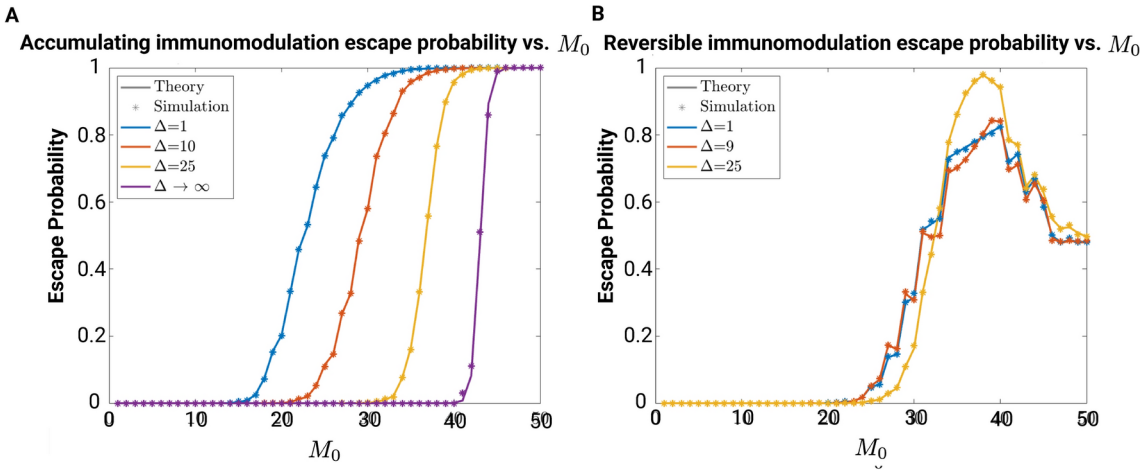

Fig. 5. Escape probability under accumulating and reversible immunomodulation landscapes. Simulation estimates of escape probability are compared alongside the theoretical results (SI Sec. S8.1) for (**A**) accumulating and (**B**) reversible immunomodulation. For each curve, a total of 10^4 stochastic simulations were used to obtain an average (in all cases, f is used according to (3) with $r = 0.005$, $\delta = 1$, $\alpha = \beta = 1$).

reversible and accumulating immunomodulation landscapes across a range of partition intervals $\Delta = \delta_{i+1} - \delta_i$ and initial immunomodulation values M_0 (Fig. 5).

Application to clinical data

The above nonlinear birth-death processes illustrate how the particular mechanism underlying T cell impairment can lead to variable population dynamical responses. Given this, we next aimed to apply our framework to large-cohort studies in order to quantify which frameworks were more applicable for explaining observed distributions of cancer progression times, in addition to predicting the corresponding extent of immune impairment. We reasoned that the application of our model to subsequent cancer progression events would provide one way of assessing immune impairment underlying repeated disease escape, given the absence of detailed time-course descriptions tracking the population sizes of non-malignant cells in a small tumor microenvironment. Two excellent patient cohorts exist that contain information on time from diagnosis to first progression and subsequent inter-progression times. These datasets comprise progression-free survival times for 3505 bladder cancer patients following diagnosis and cystectomy and 4181 breast cancer patients[41–44]. In all cases, absence of metastatic disease was confirmed at the time of detection.

Toward that end, we calculated the empirical distributions for the k^{th} inter-progression times. These distributions were then compared to our theoretical results by fitting tumor escape times assuming dynamic (constant), reversible, and accumulating landscapes. The extent of immunomodulation M, along with α and δ , were used as free parameters for each inter-progression event (Fig. 6). As one might expect, reasonable fits for bladder and breast cases required distinct α and δ parameters for each cancer subtype, although in our fitting procedure we required that the optimized parameter choices be fixed for each family of progression curves within a given cancer subtype. We then identified the least-squares best-fit curves and corresponding M values while keeping the remaining dynamical parameters (r and β) fixed across all times for a given cancer type. In particular, the value of M was fitted in the static immunomodulation case, while in the active cases we fitted the fixed increment $\Delta M \equiv M_{i+1} - M_i$ having fixed initial value ($M_0 = 5$). This procedure was applied assuming the active, reversible, and accumulating immunomodulation cases for both bladder and breast cancer (Fig. 6; MSE in SI Fig. S13). Furthermore, our parameter identifiability analysis (SI Fig. S15) highlights the correlations between key model parameters, indicating potential dependencies that may influence parameter estimation and model robustness.

Selection of M_0 was initially guided by the relevant parameter regimes realized from the theoretical analysis. In particular, the theoretical investigation of Eq. (11), (see SI Sec. S7.2 for full details) demonstrates trivial model escape behavior whenever $M > \delta/r$. Thus, $M_0 \in (0, \delta/r)$ provides a parameter regime that permits stable population equilibria. Given this finding, selection of small integer-valued $M_0 < \delta/r$ allows the dynamics of M to fluctuate considerably in a range permitting stable population equilibria. Therefore, this choice explores feasible changes in reversible and accumulating immunomodulation landscapes prior to reaching immune escape. Additionally, MSE values for M_0 ranging from 2 to 7 were evaluated based on the average across all breast cancer progression stages all exhibit comparable MSE values, we opted to select $M_0 = 5$ for which MSE was minimized (SI Fig. S14A).

To identify an order-of-magnitude choice for the increment ΔM per change in 10 tumor cells for all simulations of immunomodulatory landscapes for both breast and bladder cancer, we conducted a sensitivity analysis by varying the increment value from 10^{-4} to 0.2 in the breast cancer cohort. Our results demonstrated

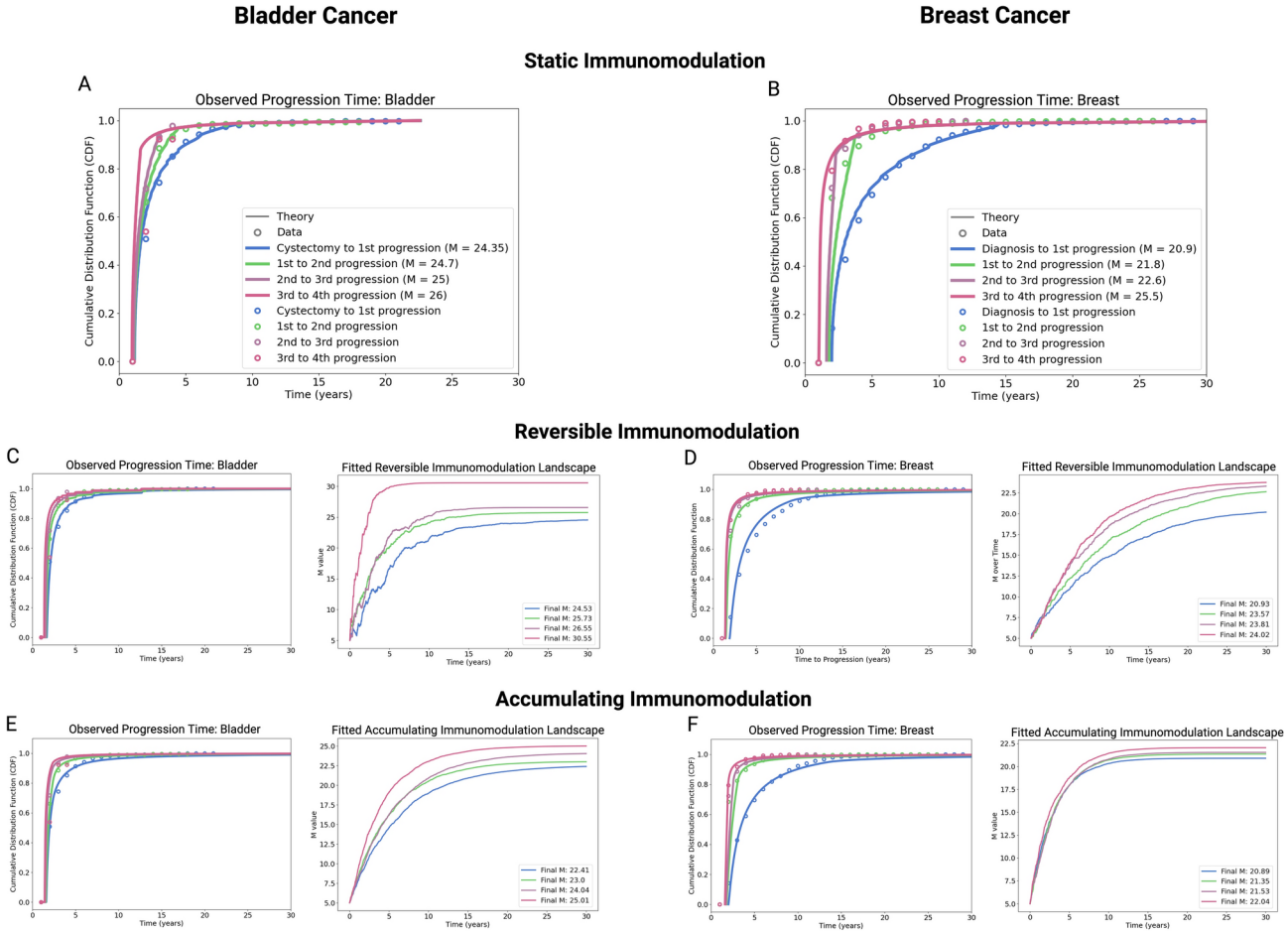

Fig. 6. The mathematical model was applied to clinical data for bladder cancer (**A**) and breast cancer (**B**) to estimate the immunomodulatory parameter M under a constant immunomodulatory landscape. The parameters for all cases were set at the optimal values of $r = 0.01$ and $\beta = 1$, which were found to be consistent across all stages of progression in both cancer types. For bladder cancer, the fitted parameters were $\alpha = 0.81$ and $\delta = 0.895$, while for breast cancer, $\alpha = 0.81$ and $\delta = 0.82$. The model was also examined under a reversible immunomodulatory landscape, with $\alpha = 0.75$ and $\delta = 0.99$ for bladder cancer, and $\alpha = 0.85$ and $\delta = 0.85$ for breast cancer. Additionally, an accumulating immunomodulatory landscape was analyzed, as represented in Panels E and F. For bladder cancer (**E**), $\alpha = 0.93$ and $\delta = 0.95$, and for breast cancer (**F**), $\alpha = 0.85$ and $\delta = 0.85$. The initial value of M in both the accumulating and reversible cases was set to 5, with M incrementing by 0.01 in response to an increase of 10 cells in the population. These parameters were identified by minimizing the mean squared error (MSE) between the model's predictions and clinical data and were assessed for parameter identifiability. The analysis (Fig. S14) highlights practical identifiability challenges, as multiple parameter combinations can yield similar model predictions. While some parameters are well-constrained, strong correlations among immunomodulatory parameters indicate structural non-identifiability, suggesting the need for additional empirical constraints to refine parameter estimation. Although the parameters differ between cancer types, they remain consistent across the stages of progression within each type.

comparable mean squared error (MSE) values for small (0.005 and 0.01) increments (SI Fig. S14B), while there were increases in MSE for very small ($\sim 10^{-4}$) and large (~ 0.1) increment values. We remark that the limit as the increment approaches zero corresponds to the active immunomodulation case without a dynamic landscape. Larger ΔM increments result in drastic jumps in immune impairment and hence deliver fewer values of M that are compatible with stable equilibrium tumor sizes, therefore resulting in rapid immune escape.

Our findings suggest that incorporation of the dynamic immunomodulation landscapes improves model fit for both breast and bladder cancer. Reversible immunomodulation outperforms accumulating immunomodulation in explaining observed progression for both breast and bladder cancer, although this finding is more pronounced in breast. This relative improved fit in breast cancer may reflect the extent to which reversible immunomodulation is more pronounced in this cancer subtype. It is also possible that multiple immunomodulatory mechanisms are at play, either in combination or over different progression intervals, which was not systematically evaluated in our present study. For bladder cancer, our findings suggest that immune inhibition exhibits persistently elevated levels relative to breast, which could be a result of increased stromal cell abundance or heightened

immunosuppressive signaling. Additionally, greater variability observed in late-stage progression (SI Fig. S13) can also contribute to higher MSE. Lastly, fits for breast cancer were performed on a larger patient dataset (4181 cases in breast versus 3505 for bladder cancer), thereby providing a more comprehensive representation of breast cancer population dynamics.

Overall, all three model descriptions struggle to well-explain advanced progression in bladder cancer, which may be a consequence of bladder cancer disease heterogeneity, particularly after multiple progression events. This finding contrasts with breast cancer, where the diminishing enhancements in immunomodulation over subsequent progression events appear to result in more predictable dynamics and improved model fit.

Despite the reversible case being the best at explaining both disease types, the time evolution of M in the reversible case exhibits gradual increases in time which closely mimic the accumulating case. Within a given cancer subtype, the immunomodulatory signal strength increases from one progression step to the next. In comparing our results for a given model across cancer types, we find uniformly higher immune inhibitory values consistently occur in bladder cancer. This finding offers one plausible explanation for its relative aggressiveness from the standpoint of adaptive immune escape, which is consistent with observed immune escape in bladder cancer[46,47]

In restricting our attention to reversible immunomodulation (Fig. 6C-D), both breast and bladder cancer are predicted to exhibit increasing immunomdulation landscapes as a function of progression events. We observe that the greatest jumps in the immunomodulation landscape are predicted to occur during early (first and second) and late (third and fourth) progression events for bladder cancer. This contrasts with breast cancer, which appear to demonstrate diminishing enhancements in immunomodulation over each subsequent progression event. In summary, our approach provides one method of mapping observed differences in relative cancer escape times to the underlying nature and extent of immune escape resulting from T cell recognition impairment.

Discussion

Recent successes in cancer immunotherapy have delivered improved disease-free survival by enhancing the anti-tumor killing effect of T cells. However, it is known that the tumor-immune interaction may lead to cancer escape, elimination, or an equilibrium state wherein the immune system keeps cancer division under control. We developed a stochastic population dynamical model to account for both the role of immune impairment on cancer escape and also the nontrivial influence of fluctuations on cancer elimination in the regime of small population sizes. Our generalized theoretical framework, together with the diffusion approximation and quantification of the likelihood and timing of escape, is applicable to other biological contexts where populations undergo nonlinear birth and death.

In a model of balanced tumor growth and death resulting in stable cancer equilibrium states at small population sizes, ultimate cancer escape is infeasible if T cell impairment results passively from the mere presence of surrounding stromal cells. This led us to extend our model to account for active immunomodulation based on the population size of cancer and inhibitory cells. The extended model can flexibly describe a variety of active impairments, including in the setting where inhibitory cells vary dynamically in response to the number of (stochastically fluctuating) cancer cells. In our application to repeated cancer progression events, our model fits suggest the relative suitability of a reversible immune impairment in the tumor microenvironment for both breast and bladder cancer.

Of course, many additional factors, including treatment course, cancer heterogeneity, and individual patient characteristics, all play an important role in determining progression times. Our foundational model offers a minimalistic description of how varying immune impairment alone can result in disease progression, which already does a reasonable job in fitting families of these distributions. Variation in the extent to which each subsequent progression event altered the predicted immune inhibitory landscape provides one way where such a model can be employed to plan aggressive treatment vs. conservative management. The finding that a reversible immunomodulation framework best explains the empirical data bears potential implications for optimal treatment and also offers hope that the immune microenvironment can be "coaxed" into a state that favors cancer elimination. Such results are of clinical significance and require further experimental follow-up.

Our approach developed a family of model modifications, wherein additional features are incrementally added with the intention of sequentially increasingly realistic and complex features into a dynamical description of tumor immunomodulation. This bottom-up approach has the benefit of incorporating stepwise complexity while also preserving foundational theoretical understanding. In practice, a direct calibration of the more complicated (reversible and accumulating immunomodulatory) model modifications would benefit from additional parameter estimation. In all modifications, cancer growth rates r can utilize previously reported estimates of division rates, or can be measured using standard (e.g., Ki-67) assays. Similarly, well-established CD8+ T cell killing assays that vary the effector-to-target ratios in the absence of stromal or inhibitory influences can inform the selection of the maximal immune killing rates δ. Stromal cell abundance M can be measured by estimating the density of nonmalignant cells in an *in vitro* co-culture with the cancer subtype of interest. In this empirical context, α and β, which capture the effects of stromal and immune interactions on tumor dynamics, could be estimated by relating observed decreases in killing rates below δ to an experimentally variable number of tumor and stromal cells.

When applying our model to cancer incidence data, we restricted our attention to the case of minimal step size for changes in immunomodulation, both in terms of the cell population size at which the modulation changed and the magnitude of the change in immunomodulation. This simplification represents a 'maximally responsive' system that preserves the key dynamical features of the immunomodulatory landscape modification in question. In the future, explicit parameter estimation from experimental data will improve model accuracy for a given cancer subtype under study. For example, *in vitro* CD8+ T cell killing assays could be used to distinguish between active and passive cases by estimating the killing rate with variable numbers of stromal cells while keeping the

tumor population size fixed. Similar experimental assays could also be used to estimate the extent to which (reversible and accumulating) immunomodulatory landscapes alter the per-cell killing rate by concomitantly varying both the initial tumor and stromal cell abundances. The advantage of including partition interval Δ is that it allows variability in the extent to which the immunomodulatory landscape can be coarsegrained. Variable partitions can thus be used to match the model landscape with observed changes in immunomodulation at each cancer cell size observed in *in vitro* investigation.

Our model's ability to capture dynamic tumor-immune interactions in the setting of variable immunomodulation offers a computational tool that can complement the design and optimization of immunotherapies as well as the relative effects of interventions that target immunomodulators in the tumor microenvironment. For example, the framework could be used once calibrated with *in vitro* experiments to predict the effects of checkpoint inhibitors, T cell-based therapies, or other immunomodulatory treatments under different tumor microenvironment conditions. Similarly, model specialization to account for relevant stromal cells, including cancer-associated fibroblasts, regulatory T cells, and myeloid-derived suppressor cells, will be useful for identifying the most important contributors to immune escape. Such a prioritization could then be used to identify immunotherapeutic approaches to recover T cell recognition. Moreover, iterative simulation to identify the effects of distinct immunotherapy dosing schedules could be implemented to find those treatment regimes that maximize cancer elimination probability. Extending the model to incorporate patient-specific heterogeneity and spatial dynamics could further enhance its utility in personalized medicine, enabling tailored treatment strategies that reflect the unique tumor-immune interactions of individual patients.

As mentioned above, one strength of this modeling approach is the relative simplicity of casting immune impairment as a nonlinear term in the cancer death rate. Such an approach, while amenable to analytic characterization, does not explicitly track the complex dynamics involving multiple cell types, signaling molecules, and feedback mechanisms, which are coarse-grained into the net growth parameter directly. In particular, the detailed dynamics of T cell activation, proliferation, and suppression are not explicitly modeled, nor are other immune populations tracked. Population dynamics are determined assuming homogeneous interactions between the cancer and immune cells, while in reality, spatial effects (such as T cell exclusion) may distort this idealized representation in solid malignancies. This model does not track distinct tumor and T cell clonotypes and consequent co-evolution process. Such an extension could be considered by assigning clone-specific parameter values, as has been the focus of prior studies[11,13]. We considered a dynamical immunomodulation parameter, but it is also possible that the other governing parameters are dynamic variables in time. Lastly, and though a relatively lenient assumption, the diffusion approximation is limited to describing Lipschitz birth and death rates (SI. Sec. S6).

The model's simplifying assumptions may impact the accuracy of predictions for solid tumors. Specifically, we assumed tumor homogeneity, which overlooks the variability in (epi)genetic, phenotypic, and microenvironmental characteristics both within and across tumors. This simplification may lead to an incomplete representation of immune-mediated control, particularly in heterogeneous tumors, where subclonal diversity and differential responses to immunomodulation are critical. Additionally, the model does not account for spatial dynamics, such as gradients of immune infiltration, localized suppression, and cell-cell interactions, which are vital in shaping tumor progression. Neglecting these spatial effects may underestimate localized immune escape or infiltration patterns, particularly in solid malignancies exhibiting significant spatial heterogeneity.

Parameter identifiability is a nontrivial concern of numerical implementation of complex model dynamics[48], made more difficult by the effects of noisy dynamics[49]. Our analysis indicated that while parameters r (tumor progression rate) and M (stromal cell abundance) are structurally and practically identifiable, other parameters (α, β, and δ) each exhibit varying degrees of practical non-identifiability. This is particularly evident in cases where immune activation and suppression processes occur simultaneously, leading to strong correlations between α and δ. Additionally, conditions with fluctuating immune responses or rapid changes in the tumor microenvironment exacerbate the identifiability issues, as β mediates the immunomodulatory landscape and is highly correlated with both α and δ, making independent estimation of these parameters challenging. These overlapping contributions result in broad posterior distributions and significant correlations among the immunomodulatory parameters.

In the future, follow-up empirical methods could help to improve this issue by further constraining poorly identified parameters. For example, targeted experimental studies that systematically vary stromal and immune cell abundances could provide direct insights into the effects captured by α and β. Additionally, longitudinal data tracking tumor-immune interactions at high temporal resolution could enhance the identifiability of parameters like δ, particularly when coupled with advanced techniques like profile likelihood analysis or hierarchical Bayesian modeling[50]. Despite these limitations, the model provides valuable qualitative insights into tumor-immune dynamics and this work represents the first stochastic description and corresponding analytic theory of tumor immune-mediated dormancy. Future work could address these issues by incorporating spatially resolved and heterogeneity-aware frameworks, such as agent-based or multi-compartmental models, and by extending the clinical dataset for bladder cancer to enhance parameter estimation and predictive robustness.

Data availability

All data generated or analysed during this study are included in this published article [and its supplementary information files].

Received: 28 August 2024; Accepted: 20 February 2025
Published online: 01 March 2025

References

1. Michor, F., Iwasa, Y. & Nowak, M. A. Dynamics of cancer progression. *Nature reviews cancer* **4**, 197–205 (2004).
2. Iwasa, Y., Nowak, M. A. & Michor, F. Evolution of resistance during clonal expansion. *Genetics* **172**, 2557–2566 (2006).
3. Komarova, N. Stochastic modeling of drug resistance in cancer. *Journal of theoretical biology* **239**, 351–366 (2006).
4. Hata, A. N. et al. Tumor cells can follow distinct evolutionary paths to become resistant to epidermal growth factor receptor inhibition. *Nature medicine* **22**, 262–269 (2016).
5. Diaz, L. A. Jr. et al. The molecular evolution of acquired resistance to targeted egfr blockade in colorectal cancers. *Nature* **486**, 537–540 (2012).
6. Couzin-Frankel, J. Cancer immunotherapy. *Science* **342**, 1432–1433 (2013).
7. Whiteside, T. L. Immune suppression in cancer: effects on immune cells, mechanisms and future therapeutic intervention. *Seminars in cancer biology* **16**, 3–15 (2006).
8. Schreiber, R. D., Old, L. J. & Smyth, M. J. Cancer immunoediting: integrating immunity's roles in cancer suppression and promotion. *Science* **331**, 1565–1570 (2011).
9. George, J. T. & Levine, H. Stochastic modeling of tumor progression and immune evasion. *Journal of theoretical biology* **458**, 148–155 (2018).
10. Palmer, S., Albergante, L., Blackburn, C. C. & Newman, T. Thymic involution and rising disease incidence with age. *Proceedings of the National Academy of Sciences* **115**, 1883–1888 (2018).
11. George, J. T. & Levine, H. Implications of tumor-immune coevolution on cancer evasion and optimized immunotherapy. *Trends in Cancer* **7**, P373-383 (2021).
12. George, J. T. & Levine, H. Sustained coevolution in a stochastic model of cancer-immune interaction. *Cancer research* **80**, 811–819 (2020).
13. George, J. T. & Levine, H. Optimal cancer evasion in a dynamic immune microenvironment generates diverse post-escape tumor antigenicity profiles. *Elife* **12**, e82786 (2023).
14. Turajlic, S. et al. Tracking cancer evolution reveals constrained routes to metastases: Tracerx renal. *Cell* **173**, 581–594 (2018).
15. Jamal-Hanjani, M. et al. Tracking the evolution of non-small-cell lung cancer. *New England Journal of Medicine* **376**, 2109–2121 (2017).
16. McGranahan, N. & Swanton, C. Clonal heterogeneity and tumor evolution: past, present, and the future. *Cell* **168**, 613–628 (2017).
17. Lakatos, E. et al. Evolutionary dynamics of neoantigens in growing tumors. *Nature genetics* **52**, 1057–1066 (2020).
18. Giancotti, F. G. Mechanisms governing metastatic dormancy and reactivation. *Cell* **155**, 750–764 (2013).
19. Yeh, A. C. & Ramaswamy, S. Mechanisms of cancer cell dormancy-another hallmark of cancer?. *Cancer research* **75**, 5014–5022 (2015).
20. Wang, H.-F. et al. Targeting immune-mediated dormancy: a promising treatment of cancer. *Frontiers in oncology* **9**, 498 (2019).
21. Dunn, G. P., Old, L. J. & Schreiber, R. D. The three es of cancer immunoediting. *Annu. Rev. Immunol.* **22**, 329–360 (2004).
22. MacKie, R. M., Reid, R. & Junor, B. Fatal melanoma transferred in a donated kidney 16 years after melanoma surgery. *New England Journal of Medicine* **348**, 567–568 (2003).
23. Koebel, C. M. et al. Adaptive immunity maintains occult cancer in an equilibrium state. *Nature* **450**, 903–907 (2007).
24. Summers, M. A., McDonald, M. M. & Croucher, P. I. Cancer cell dormancy in metastasis. *Cold Spring Harbor Perspectives in Medicine* **10** (2020).
25. Molon, B., Calì, B. & Viola, A. T cells and cancer: how metabolism shapes immunity. *Frontiers in immunology* **7**, 20 (2016).
26. Amedei, A. et al. Ex vivo analysis of pancreatic cancer-infiltrating t lymphocytes reveals that eno-specific tregs accumulate in tumor tissue and inhibit th1/th17 effector cell functions. *Cancer Immunology, Immunotherapy* **62**, 1249–1260 (2013).
27. Cao, X. et al. Granzyme b and perforin are important for regulatory t cell-mediated suppression of tumor clearance. *Immunity* **27**, 635–646 (2007).
28. Whiteside, T. L. The role of regulatory t cells in cancer immunology. *ImmunoTargets and therapy* 159–171 (2015).
29. Czekay, R.-P., Cheon, D.-J., Samarakoon, R., Kutz, S. M. & Higgins, P. J. Cancer-associated fibroblasts: mechanisms of tumor progression and novel therapeutic targets. *Cancers* **14**, 1231 (2022).
30. Glabman, R. A., Choyke, P. L. & Sato, N. Cancer-associated fibroblasts: Tumorigenicity and targeting for cancer therapy. *Cancers* **14**, 3906 (2022).
31. Hatziioannou, A., Alissafi, T. & Verginis, P. Myeloid-derived suppressor cells and t regulatory cells in tumors: unraveling the dark side of the force. *Journal of Leukocyte Biology* **102**, 407–421 (2017).
32. Srivastava, M. K., Sinha, P., Clements, V. K., Rodriguez, P. & Ostrand-Rosenberg, S. Myeloid-derived suppressor cells inhibit t-cell activation by depleting cystine and cysteine. *Cancer research* **70**, 68–77 (2010).
33. Monu, N. R. & Frey, A. B. Myeloid-derived suppressor cells and anti-tumor t cells: a complex relationship. *Immunological investigations* **41**, 595–613 (2012).
34. Huang, B. et al. Gr-1+ cd115+ immature myeloid suppressor cells mediate the development of tumor-induced t regulatory cells and t-cell anergy in tumor-bearing host. *Cancer research* **66**, 1123–1131 (2006).
35. Liu, C. et al. Expansion of spleen myeloid suppressor cells represses nk cell cytotoxicity in tumor-bearing host. *Blood* **109**, 4336–4342 (2007).
36. Wilkie, K. P. & Hahnfeldt, P. Mathematical models of immune-induced cancer dormancy and the emergence of immune evasion. *Interface Focus* **3**, 20130010 (2013).
37. Wilkie, K. P., Hahnfeldt, P. & Hlatky, L. Using ordinary differential equations to explore cancer-immune dynamics and tumor dormancy. *bioRxiv* 049874 (2016).
38. Scharping, N. E. et al. The tumor microenvironment represses t cell mitochondrial biogenesis to drive intratumoral t cell metabolic insufficiency and dysfunction. *Immunity* **45**, 374–388 (2016).
39. Watson, M. J. et al. Metabolic support of tumour-infiltrating regulatory t cells by lactic acid. *Nature* **591**, 645–651 (2021).
40. Valkenburg, K. C., de Groot, A. E. & Pienta, K. J. Targeting the tumour stroma to improve cancer therapy. *Nat Rev Clin Oncol* **15**, 366–381 (2018).
41. Newton, P. K. et al. Breast cancer modelling (2015). Website online available; accessed at 8/14/2024.
42. Newton, P. K. et al. Spatiotemporal progression of metastatic breast cancer: a markov chain model highlighting the role of early metastatic sites. *npj Breast Cancer* **1**, 15018. https://doi.org/10.1038/npjbcancer.2015.18 (2015).
43. Hasnain, Z. et al. Bladder cancer modelling (2019). Website online available; accessed at 8/14/2024.
44. Hasnain, Z. et al. Machine learning models for predicting post-cystectomy recurrence and survival in bladder cancer patients. *PLOS ONE* **14**, 1–15. https://doi.org/10.1371/journal.pone.0210976 (2019).
45. Hao, Z. et al. Landscape of myeloid-derived suppressor cell in tumor immunotherapy. *Biomarker Research* **9**, 1–28 (2021).
46. Gil-Julio, H. et al. Tumor escape phenotype in bladder cancer is associated with loss of hla class i expression, t-cell exclusion and stromal changes. *International Journal of Molecular Sciences* **22**, 7248 (2021).
47. Yang, Z. et al. Immune escape mechanisms and immunotherapy of urothelial bladder cancer. *Journal of clinical and translational research* **7**, 485 (2021).
48. Browning, A. P., Warne, D. J., Burrage, K., Baker, R. E. & Simpson, M. J. Identifiability analysis for stochastic differential equation models in systems biology. *Journal of the Royal Society Interface* **17**, 20200652 (2020).
49. Martina-Perez, S., Simpson, M. J. & Baker, R. E. Bayesian uncertainty quantification for data-driven equation learning. *Proceedings of the Royal Society A* **477**, 20210426 (2021).

50. Raue, A. et al. Structural and practical identifiability analysis of partially observed dynamical models by exploiting the profile likelihood. *Bioinformatics* **25**, 1923–1929 (2009).

Acknowledgements
We thank Herbert Levine for helpful discussions on modeling cancer immune-mediated dormancy. JTG was supported by the Cancer Prevention Research Institute of Texas (RR210080), and the National Institute of General Medical Sciences of the NIH (R35GM155458). JTG is a CPRIT Scholar in Cancer Research.

Author contributions
P.S. designed the research, contributed new analytic equations, performed the research, analyzed the data, and wrote the manuscript. Z.S.G performed the research, analyzed the data, and wrote the manuscript. J.T.G. conceived of and designed the research, analyzed the data, contributed new analytic equations, and wrote the manuscript. All authors have approved the final article.

Declarations

Competing interests
The authors declare no competing interests.

Additional information
Supplementary Information The online version contains supplementary material available at https://doi.org/10.1038/s41598-025-91396-z.

Correspondence and requests for materials should be addressed to J.T.G.